Generation of a 20 GHz train of subpicosecond pulses with a stabilized optical-frequency-comb generator

Shijun Xiao,* Leo Hollberg, and Scott A. Diddams

Time and Frequency Division, National Institute of Standards and Technology, 325 Broadway, Boulder, Colorado 80305, USA

**Corresponding author: sxiao@boulder.nist.gov*

Received September 16, 2008; revised October 30, 2008; accepted November 4, 2008; posted November 19, 2008 (Doc. ID 101552); published December 24, 2008

With a modulator-based 10 GHz optical-frequency-comb generator at 1.55 μm, we report a 20 GHz repetitive train of optical pulses as short as 450 fs. The timing stability of the 20 GHz pulses, in addition to the phase for optical-comb modes, shows a strong dependence on the relative frequency detuning between the comb generator's cavity and the seed cw laser. With a new and simple scheme, the comb generator's cavity resonance was locked to a narrow-linewidth seed laser within an estimated optical-frequency range $\leqslant$6 MHz, enabling high-fidelity 20 GHz subpicosecond pulses and stable optical-frequency-comb generation for indefinite periods.

OCIS codes: 120.3930, 120.3940, 320.5550, 320.5390.

Extensive work has been carried out on the generation of high-speed (e.g., 10 GHz) picosecond pulses at 1.55 μm that have low timing jitter. Some of the techniques include passively mode-locked solid-state lasers [1] as well as actively mode-locked fiber [2,3] and semiconductor lasers [4]. To the best of our knowledge, these techniques do not directly produce subpicosecond pulses at rates over 10 GHz, and extensive effort is often required to obtain <10 fs residual timing jitter in actively mode-locked fiber and semiconductor lasers. An alternative approach, which we explore in this Letter, involves pulse generation with the combination of a continuous wave (cw) laser that seeds a resonant Fabry–Perot (F–P) electro-optical phase modulator, the so-called optical-frequency-comb generator (OFCG) [5]. This technique has the advantages of simplicity, large wavelength tunability, and precise and straightforward control of the associated optical-frequency comb. A unique feature of the OFCG is that its output consists of a pair of interleaved optical pulse trains [5–8]. This is beneficial for the generation of a pulse train at a repetition rate double that of the modulation frequency (e.g., 20 GHz pulse train for a 10 GHz modulation), but the relative positions of the interleaved trains must be precisely controlled for high-fidelity 20 GHz pulses. For Fourier frequencies from 1 Hz to 10 MHz, we demonstrated sub-10 fs integrated phase timing jitter at 10 GHz with the OFCG [8]. In this Letter, we analyze the output of an OFCG that produces a 20 GHz pulse train at 1.55 μm. Autocorrelation measurements show that pulses as short as 450 fs can be produced directly from the OFCG, which is near the Fourier transform limit. A simple approach is introduced for stabilization of the OFCG's cavity relative to the cw seed laser. The impact of this stabilization on the resulting relative timing positions between the two interleaved pulse trains is analyzed, which indicates that both stable 20 GHz pulses and stable 10 GHz optical frequency combs can be maintained over indefinite periods of time. These results should be relevant to several application areas, including precision frequency metrology and spectroscopy [5], high-fidelity line-by-line femtosecond pulse shaping [9], and high-speed fiber communication [9].

Figure 1 shows the principle of the OFCG, which consists of a $LiNbO_3$ waveguide phase modulator in the structure of an F–P cavity [10]. The microwave modulation frequency f_m=10 GHz is four times the free spectral range (FSR) of the F–P cavity. The OFCG's temporal output depends on the relative frequency offset $\boldsymbol{\delta\nu}$ between the seed laser ($\boldsymbol{\nu}_o$) and the F–P cavity resonance ($\boldsymbol{\nu}_{\mathbf{cavity}}$). The temporal output of the OFCG consists of two interleaved 10 GHz pulse trains with nearly identical pulses (see Fig. 1). A pulse is produced on the rising and the falling slopes of the sinusoidal microwave modulation as the effective cavity length is brought into resonance with the seed laser [8]. For $\boldsymbol{\delta\nu}$=0, the two 10 GHz inter-

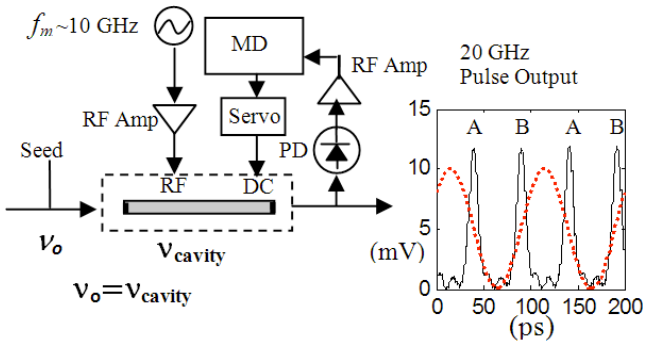

Fig. 1. (Color online) Schematic principle of the OFCG for the generation of short pulses at a high repetition rate. $\boldsymbol{\nu}_o$ is the frequency of the optical cw seed laser. $\boldsymbol{\nu}_{\mathrm{cavity}}$ is the OFCG cavity resonance frequency. MD is a microwave detector diode, and PD is a high-speed photodiode. The dotted line represents the sinusoidal modulation; pulses measured directly out of the PD are generated at every zero modulation phase, and the pulses labeled A and B represent the two pairs of interleaved 10 GHz pulse trains.

leaved pulse trains appears as a single 20 GHz pulse train. The pulse intensity has a Lorentzian shape, and the intensity full width at half maximum (FWHM) is $1/(F\beta f_m)$ [8], where $F=60$ is the finesse of the F–P cavity and β is the modulation index. Figure 2(a) shows the optical power spectrum directly at the OFCG output, when seeded with a cw fiber laser centered at 1535 nm. The comb spans about 6 THz, and the optical power decays ~0.12 dB per comb element (1.5 dB/nm). This corresponds to a modulation index β of 1.2 π, and the calculated pulse width is 0.44 ps. Figure 2(b) shows the intensity autocorrelation trace of the pulse train from the OFCG. Here we have employed a semiconductor optical amplifier (SOA) to amplify the OFCG output prior to autocorrelation. The solid curve is the experimental autocorrelation trace, and the dotted curve is the theoretical fit for a Lorentzian pulse. The wings of the experimental data are attributed to the uncompensated higher-order dispersion of the SOA. The FWHM of the intensity autocorrelation is 0.9 ps, which corresponds to a pulse width of about 0.45 ps, in agreement with the theory.

Long-term stability characterization is achieved by analyzing the microwave spectrum of the OFCG output. In these measurements a cw fiber laser centered at 1550 nm was used to seed the OFCG with a modulation index $\beta \sim \pi$. Additional optical amplification was not employed. Figure 3(a) shows the spectrum for $\boldsymbol{\delta\nu}=0$. The optical power to the photodiode was −9.3 dBm, yielding a microwave power at 20 GHz of −42 dBm. The 10 GHz power is suppressed to >40 dB below this level. The residual 10 GHz power is attributed to slight power and spectral imbalances between the two interleaved 10 GHz pulse trains. Figure 3(b) shows the microwave power at 10 and 20 GHz, respectively, as functions of the normalized frequency detuning ($|\boldsymbol{\delta\nu}|$/FSR). The 10 GHz power suppression is very sensitive to small variations (tens of megahertz) of $\boldsymbol{\delta\nu}$ near zero while the microwave power at 20 GHz is insensitive. In Fig. 1 we present our stabilization scheme for locking $\boldsymbol{\delta\nu}$, which is different from previous approaches [7,11] that proposed using the phase of the f_m harmonic but did not verify long-term stabilization. In our case, we take the advantage of the fact that the power of the f_m harmonic

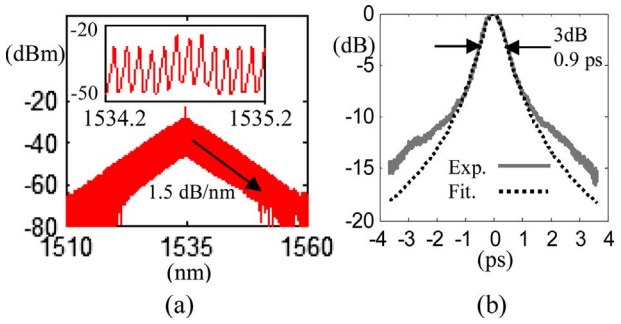

Fig. 2. (Color online) (a) Optical spectrum of the OFCG output. The spectral resolution was 0.02 nm. The discrete 10 GHz (~0.08 nm) frequency comb lines are resolved, indicated by the inset. (b) Intensity autocorrelation of the 20 GHz pulse. The dotted curve is a Lorentzian fit.

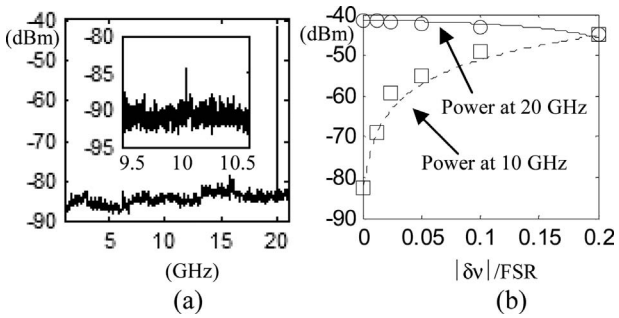

Fig. 3. (a) Microwave spectrum of the 20 GHz output pulse. The resolution bandwidth was 100 kHz. The spectrum noise floor is that of the spectrum analyzer. (b) Power at 10 GHz (dashed and square curve) and 20 GHz (solid and circle curve) for different frequency detunings. The curves (dashed and solid) are calculated values, and the discrete points (square and circle) are experimental measurements.

almost vanishes at $\boldsymbol{\delta\nu}=0$, which provides a strong and interferometrically sensitive signal to control the relative time offset between the two interleaved pulse trains. The servo system is configured to minimize the microwave power detected at 10 GHz, thereby forcing strictly equal temporal spacing between the two interleaved 10 GHz pulse trains.

We characterize the long-term stability of the output 20 GHz pulse train by analyzing the power of the 10 and 20 GHz microwave harmonics. The input seed laser power was 80 mW with a stability ±1%, and the total output optical power was about 0.25 mW. One half of the optical power was used for the servo loop, and the other half was used for stability characterization. Figure 4(a) shows the time evolution of the microwave power for the case without servo (curves labeled "Unlocked") and the case with servo (curves labeled "Locked"). At the beginning of the measurement, $\boldsymbol{\delta\nu}$ was tuned to be zero, and the microwave power at 10 GHz was about −82 dBm. For the case without servo, after 40 h, the microwave power at 10 GHz increased to −49 dBm while the microwave power at 20 GHz decreased by a few decibels. With the servo engaged, the microwave power at 10 GHz is minimized and stays between −80 and −84 dBm. The

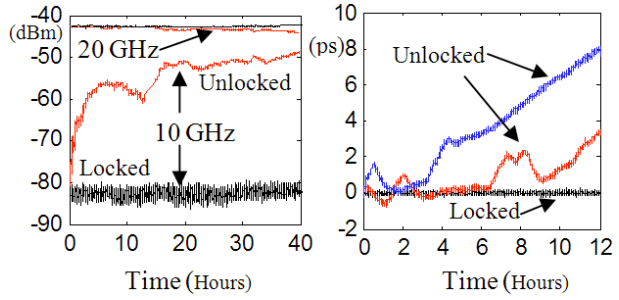

Fig. 4. (Color online) (a) Time evolution of the microwave power from the spectrum of the output pulse. The data were recorded at 2 samples/min. (b) Fluctuation of the relative timing delay (offset from 50 ps) between the two interleaved 10 GHz pulses. The data were recorded at 10 samples/min.

measurement noise floor was −90 dBm. Correspondingly, the microwave power at 20 GHz is stable at −42.5 dBm (±0.1 dB).

The timing quality of the 20 GHz pulse train can be significantly degraded for small shifts of $\boldsymbol{\delta\nu}$ away from zero. This is evidenced by the change of the relative timing delay between the two interleaved 10 GHz pulses, as given by

$$\Delta t = \frac{1}{\pi f_m} \times \sin^{-1}\left(\frac{2\pi|\delta\upsilon|}{\beta \times \mathrm{FSR}}\right) \approx \frac{1}{\pi f_m}\frac{2\pi|\delta\upsilon|}{\beta \times \mathrm{FSR}}. \quad (1)$$

As an example, we see that with $\beta \sim \pi$, Δt can be changed by about 0.6 ps for $\boldsymbol{\delta\nu}$=25 MHz ($\delta\nu$/FSR $\sim$0.01). An out-of-loop time-domain characterization of the timing stability of the 20 GHz pulse train was performed by measuring the relative timing delay between the interleaved 10 GHz pulse trains with a sampling oscilloscope, i.e., measuring the time delay between pulses A and B of Fig. 1. The results are shown in Fig. 4(b). Again, the relative timing delay was initially tuned to be half the modulation period (50 ps), corresponding to $\boldsymbol{\delta\nu}$=0. The data with the servo engaged are labeled "Locked," while the other two curves are recorded examples for the unlocked cavity. For the locked cavity, the pulse period is fixed at 50 ps and has a maximum fluctuation range of ±0.2 ps over the observation period. According to Eq. (1), the estimated cavity-locking optical frequency range is $|\boldsymbol{\delta\nu}| \leqslant 6$ MHz. The pulse period has a standard deviation of 74.2 fs after 64 averages on the oscilloscope. This level of fluctuation is essentially close to that of the time base of the sampling oscilloscope, which we measured to be 71.5 fs after 64 averages on the oscilloscope for a 10 GHz sinusoidal wave input split from the microwave signal to the OFCG. This observation indicates low residual timing jitter over long periods and complements our previous work [8].

We now consider the stability of the optical-frequency-comb teeth. Fluctuations of $\boldsymbol{\delta\nu}$ also result in fluctuations of both the power and the phase of individual optical-frequency-comb elements. For the nth comb tooth (given by $\boldsymbol{\nu}_n = \boldsymbol{\nu}_o + n \times f_m$) the relative optical power change due to the change of $\boldsymbol{\delta\nu}$ about zero is

$$\frac{\Delta P_n}{P_n} \approx \left(1 - \frac{\pi|n|}{F\beta}\right)\left(\frac{2\pi \times \delta\upsilon}{\beta \times \mathrm{FSR}}\right)^2, \quad (2)$$

where we assume $|\delta\nu|/\mathrm{FSR} \ll 1$. It is interesting to notice that the optical power does not change significantly with $\boldsymbol{\delta\nu}$. For the cavity-locking approach demonstrated above, the optical-power fluctuation is $\leqslant \sim 0.01\%$ for $|n| \leqslant 100$. On the other hand, the spectral phase fluctuations of the nth comb tooth can be more significant, as given by

$$\Delta\phi = n \times \sin^{-1}\left(\frac{2\pi \times \delta\upsilon}{\beta \times \mathrm{FSR}}\right) \approx 2n\pi\frac{\delta\upsilon}{\beta \times \mathrm{FSR}}, \quad (3)$$

where the spectral phases of the comb teeth are treated as $[0,0,\ldots]$ for $n<0$ and $n \times \pi([0,\pi,0,\pi,\ldots])$ for $n \geqslant 0$ [9] when $\boldsymbol{\delta\nu}$=0. For the cavity locking achieved above, the spectral phase change is $\leqslant 0.2\pi$ for the 100th sideband, and its power is about 15 dB lower than the combs near the seeding laser wavelength. The phase variation between two adjacent frequency combs is $\leqslant 0.002\pi$. Thus, the power and spectral phases of the optical comb should be sufficiently stable for applications that rely on the phase stability of the underlying frequency comb teeth.

In conclusion, we have used a modulator-based 1550 nm OFCG to produce a stable 20 GHz train of 450 fs pulses. We present a new stabilization scheme for locking the cavity resonance of the OFCG to a narrow-linewidth seed laser within an optical-frequency range of ≤6 MHz. Long-term (1–2 days) analysis demonstrates the importance of locking the cavity to the seed laser for the generation of high-fidelity pulses and stable optical frequency comb teeth.

We thank Bill Swann and Nate Newbury for loaning the fiber laser at 1535 nm and Andy Weiner for valuable discussions. This work was supported by National Institute of Standards and Technology (NIST) and Defense Advanced Research Projects Agency (DARPA). This paper is a contribution of an agency of the U.S. government and not subject to copyright in the U.S.

References

1. R. Paschotta, L. Krainer, S. Lecomte, G. J. Spühler, S. C. Zeller, A. Aschwanden, D. Lorenser, H. J. Unold, K. J. Weingarten, and U. Keller, New J. Phys. **6**, 174 (2004).
2. T. F. Carruthers and I. N. Duling, Opt. Lett. **21**, 1927 (1996).
3. E. Yoshida and M. Nakazawa, Electron. Lett. **34**, 1753 (1998).
4. F. Quinlan, S. Gee, S. Ozharar, and P. J. Delfyett, Opt. Lett. **31**, 2870 (2006).
5. M. Kourogi, K. Nakagawa, and M. Ohtsu, IEEE J. Quantum Electron. **29**, 2693 (1993).
6. G. M. Macfarlane, A. S. Bell, E. Riis, and A. I. Ferguson, Opt. Lett. **21**, 534 (1996).
7. M. Kato, K. Fujiura, and T. Kurihara, Appl. Opt. **44**, 1263 (2005).
8. S. Xiao, L. Hollberg, N. Newbury, and S. Diddams, Opt. Express **16**, 8498 (2008).
9. Z. Jiang, D. Leaird, C. B. Huang, H. Miao, M. Kourogi, K. Imai, and A. M. Weiner, IEEE J. Quantum Electron. **43**, 1163 (2007).
10. T. Saitoh, M. Kourogi, and M. Ohtsu, IEEE Photonics Technol. Lett. **7**, 197 (1995).
11. M. Kourogi, B. Widiyatomoko, Y. Takeuchi, and M. Ohtsu, IEEE J. Quantum Electron. **31**, 2120 (1995).